THE JOURNAL OF BIOLOGICAL CHEMISTRY VOL. 285, NO. 23, pp. 17359–17370, June 4, 2010

Identification and Functional Characterization of a Novel Mitochondrial Carrier for Citrate and Oxoglutarate in *Saccharomyces cerevisiae*[*] [S]

Received for publication, December 20, 2009, and in revised form, March 18, 2010 Published, JBC Papers in Press, April 6, 2010, DOI 10.1074/jbc.M109.097188

Alessandra Castegna[‡1], Pasquale Scarcia[‡1], Gennaro Agrimi[‡], Luigi Palmieri[‡§], Hanspeter Rottensteiner[¶], Iolanda Spera[‡], Lucrezia Germinario[‡], and Ferdinando Palmieri[‡§2]

From the [‡]Department of Pharmaco-Biology, Laboratory of Biochemistry and Molecular Biology, University of Bari, 70125 Bari, Italy, the [¶]Institut für Physiologische Chemie, Abteilung Systembiochemie, Ruhr-Universität Bochum, 44780 Bochum, Germany, and the [§]Consiglio Nazionale delle Ricerche Institute of Biomembranes and Bioenergetics, 70125 Bari, Italy

Mitochondrial carriers are a family of transport proteins that shuttle metabolites, nucleotides, and coenzymes across the mitochondrial membrane. The function of only a few of the 35 *Saccharomyces cerevisiae* mitochondrial carriers still remains to be uncovered. In this study, we have functionally defined and characterized the *S. cerevisiae* mitochondrial carrier Yhm2p. The *YHM2* gene was overexpressed in *S. cerevisiae*, and its product was purified and reconstituted into liposomes. Its transport properties, kinetic parameters, and targeting to mitochondria show that Yhm2p is a mitochondrial transporter for citrate and oxoglutarate. Reconstituted Yhm2p also transported oxaloacetate, succinate, and fumarate to a lesser extent, but virtually not malate and isocitrate. Yhm2p catalyzed only a counter-exchange transport that was saturable and inhibited by sulfhydryl-blocking reagents but not by 1,2,3-benzenetricarboxylate (a powerful inhibitor of the citrate/malate carrier). The physiological role of Yhm2p is to increase the NADPH reducing power in the cytosol (required for biosynthetic and antioxidant reactions) and probably to act as a key component of the citrate-oxoglutarate NADPH redox shuttle between mitochondria and cytosol. This protein function is based on observations documenting a decrease in the NADPH/$NADP^+$ and GSH/GSSG ratios in the cytosol of Δ*YHM2* cells as well as an increase in the NADPH/$NADP^+$ ratio in their mitochondria compared with wild-type cells. Our proposal is also supported by the growth defect displayed by the Δ*YHM2* strain and more so by the Δ*YHM2*Δ*ZWF1* strain upon H_2O_2 exposure, implying that Yhm2p has an antioxidant function.

Yhm2p is a protein of unknown function that has been found to be present in the inner mitochondrial membrane of *Saccharomyces cerevisiae* (1). This protein was shown to complement the growth defect displayed at 37 °C by *S. cerevisiae* cells lacking *ABF2*, which encodes a mitochondrial DNA-binding protein involved in mitochondrial DNA replication and recombination (1, 2). In addition, the primary structure of Yhm2p exhibits all the characteristic features of the mitochondrial carrier (MC)[3] protein family, *i.e.* a tripartite structure consisting of three tandemly repeated homologous domains of about 100 amino acids in length, each of which contains a distinct signature motif and two hydrophobic stretches that span the membrane as α-helices (for reviews see Refs. 3–5). *S. cerevisiae* possesses 35 members of this family, one of which is localized in peroxisomes and not in mitochondria. The majority of yeast MCs has been functionally characterized and shown to transport specific metabolites, nucleotides, and coenzymes across the mitochondrial membrane (for review see Ref. 6). By contrast, the substrate(s) transported by Yhm2p have not yet been discovered, and its physiological function is yet unknown.

In this study, we provide evidence that the gene product of *YMR241w*, named Coc1p and known as Yhm2p, is a citrate-oxoglutarate carrier in *S. cerevisiae*. Yhm2p was overexpressed in *S. cerevisiae*, purified, reconstituted into phospholipid vesicles, and identified for its transport properties as a novel carrier for citrate and oxoglutarate. Besides these substrates, oxaloacetate, succinate, and fumarate are also transported, to a lesser extent, by the carrier via a counter-exchange mechanism. Yhm2p operates in yeast mitochondria with transport properties similar to those observed with the recombinant protein. In addition, Δ*YHM2* cells (devoid of *YHM2*) and more so Δ*YHM2*Δ*ZWF1* cells (lacking *YHM2* and also *ZWF1* which encodes glucose-6-phosphate dehydrogenase, an important source of NADPH) exhibit a growth defect upon exposure to H_2O_2. This phenotype correlates with a decrease in the cytosolic NADPH/$NADP^+$ and GSH/GSSG ratios. This is the first time that an MC for both citrate and oxoglutarate has been identified from any organism at the molecular level. Yhm2p is suggested to have a role in increasing NADPH levels in the cytosol and to be a key component of the

* This work was supported by grants from the Ministero dell'Università e della Ricerca, the Center of Excellence in Genomics, Apulia Region, the University of Bari, and the Italian Human ProteomeNet No. RBRN07BMCT_009. This work is dedicated to the memory of Prof. Noris Siliprandi.

[S] The on-line version of this article (available at http://www.jbc.org) contains supplemental Tables S1 and S2 and Figs. S1–S4.

[1] Both authors contributed equally to this work.

[2] To whom correspondence should be addressed: Via Orabona 4, 70125 Bari, Italy. Tel.: 390805443374; Fax: 390805442770; E-mail: fpalm@farmbiol.uniba.it.

[3] The abbreviations used are: MC, mitochondrial carrier; Coc1p, citrate-oxoglutarate carrier; CTP, human citrate transport protein; DCF, 2′,7′-dichlorofluorescein; PIPES, 1,4-piperazinediethanesulfonic acid; ROS, reactive oxygen species; SC, synthetic complete medium; SM, synthetic minimal medium; YP, rich medium; DCFH-DA, dichlorodihydrofluorescein diacetate; MALDI-TOF, matrix-assisted laser desorption ionization time-of-flight; ANOVA, analysis of variance.

NADPH citrate-oxoglutarate redox shuttle that catalyzes a net transfer of NADPH reducing equivalents from the mitochondria to the cytosol.

EXPERIMENTAL PROCEDURES

Yeast Strains, Media, and Preparation of Mitochondria and Cytosol—The single and double deletion strains of YPH499 (wild type) were constructed using the PCR-mediated gene disruption technique by replacing the open reading frame of the genes under investigation with *HIS3* (7), *KanMX3* (8), or *NatMX4* (9) (see supplemental Table S1). All deletions were verified by PCR. The wild-type and deletion strains were grown at 30 °C in rich medium (YP), containing 2% bactopeptone and 1% yeast extract, synthetic complete medium (SC), or synthetic minimal medium (SM) (10) supplemented with 2% glucose or 2% acetate and auxotrophic nutrients when required. The final pH was adjusted to 4.5 (with glucose) or 6.5 (with acetate). When using solid media, 1.5% agar was added. In nearly all the experiments, yeast strains were precultured overnight in YP with 2% glucose. After washing, the cells were suspended in acetate-supplemented SC at an absorbance of 0.1 at 600 nm and grown until the early exponential phase was reached (absorbance of 0.8). These cells were incubated in the presence or absence of H_2O_2 (1 μmol $\times$ 10^7 cells) for 60 min. At this time period, the cells were harvested and centrifuged at 2500 $\times$ *g* for 10 min at 4 °C. For the preparation of the mitochondria, the pellet was resuspended in 1.2 M sorbitol and 20 mM potassium phosphate, pH 7.4, and the mitochondria were isolated as described previously (11). To prepare the cytosol, the pellet was resuspended in 0.65 M sorbitol, 0.1 M Tris-HCl, pH 8.0, and 5 mM EDTA. The cells were then disrupted by employing a cell disrupter (model Z6/40/AE/GA, Constant Systems Ltd., Daventry, UK) set at a working pressure of 207 MPa. Cellular lysates were centrifuged at 2500 $\times$ *g* for 10 min at 4 °C and then at 120,000 $\times$ *g* for 30 min at 4 °C to obtain a clear supernatant (cytosol).

Overexpression in S. cerevisiae and Purification of YHM2—The coding sequence of Yhm2p was amplified from *S. cerevisiae* genomic DNA via PCR. Forward and reverse oligonucleotide primers were synthesized corresponding to the extremities of the *YHM2* sequence with additional HindIII and BamHI sites, respectively. The reverse primer also contained 18 additional bases encoding a hexahistidine tag immediately before the stop codon. The PCR product was cloned into the yeast *pYES2* expression vector (Invitrogen) under the control of the *GAL10* promoter, and the resulting plasmid was introduced into the wild-type strain. Transformants (*YHM2-pYES2* cells) were selected for uracil auxotrophy, precultured on SC medium supplemented with 3% glycerol and 0.1% glucose for 14–16 h, diluted 35-fold in YP supplemented with the same carbon sources, and grown to mid-exponential phase. Galactose (0.45%) was added 4 h before harvesting. Mitochondria were isolated from *YHM2-pYES2* cells and solubilized in buffer A (500 mM NaCl, 10 mM PIPES, pH 7.0) containing 1.5% Triton X-100 (w/v) and 0.1 mM phenylmethylsulfonyl fluoride at a final concentration of 1 mg protein/ml. After incubation for 20 min at 4 °C, the mixture was centrifuged at 138,000 $\times$ *g* for 20 min. The supernatant (0.6 ml) was mixed for 20 min at 4 °C with 0.2 ml of nickel-nitrilotriacetic acid-agarose (Qiagen) previously equilibrated with buffer A. Afterward, the resin was packed into a column (0.5 cm internal diameter) and washed with the following buffers: B, 500 mM NaCl, 10 mM imidazole, 1.5% Triton X-100, 5% glycerol, 10 mM PIPES, pH 7.0 (2 ml); C, 300 mM NaCl, 10 mM imidazole, 1.2% Triton X-100, 1% glycerol, 10 mM PIPES, pH 7.0 (2 ml); D, 100 mM NaCl, 10 mM imidazole, 0.5% Triton X-100, 0.5% glycerol, 10 mM PIPES, pH 7.0 (2 ml); E, 100 mM NaCl, 10 mM imidazole, 0.8% Triton X-100, 10 mM PIPES, pH 7.0 (2 ml); and F, 100 mM NaCl, 20 mM imidazole, 0.4% Triton X-100, 10 mM PIPES, pH 7.0 (2 ml). Finally, pure YHM2 protein was eluted with a buffer containing 50 mM NaCl, 0.4% Triton X-100, 100 mM imidazole and 10 mM PIPES, pH 7.0 (0.9 ml).

Reconstitution into Liposomes and Transport Assays—Purified YHM2 protein was reconstituted into liposomes in the presence or absence of substrates, as described previously (12). External substrate was removed from proteoliposomes on Sephadex G-75 columns pre-equilibrated with 50 mM NaCl and 10 mM PIPES, pH 7.0 (buffer G). Transport at 25 °C was started by adding [^{14}C]citrate or [^{14}C]oxoglutarate to proteoliposomes and terminated by the addition of 30 mM pyridoxal 5′-phosphate and 10 mM bathophenanthroline, which in combination and at high concentrations inhibit the activity of several mitochondrial carriers completely and rapidly (see, for example, Refs. 13–16). In controls, the inhibitors were added with the labeled substrate. The external radioactive substrate was removed, and the radioactivity in the proteoliposomes was measured (12). The experimental values were corrected by subtracting control values. The initial transport rate was calculated from the radioactivity taken up by proteoliposomes after 1 min (in the initial linear range of substrate uptake). For efflux measurements, proteoliposomes containing 1 mM substrate were labeled with 10 μM [^{14}C]citrate by carrier-mediated exchange equilibration (12). After 60 min, the external radioactivity was removed by passing the proteoliposomes through Sephadex G-75 pre-equilibrated with buffer G. Efflux was started by adding unlabeled external substrate in buffer G, or buffer G alone, and terminated by adding the inhibitors indicated above.

Metabolite, Pyrimidine Coenzyme, and Glutathione Determinations by Mass Spectrometry—Mitochondria and cytosol were extracted with phenol/chloroform 1:1 for mass spectrometry analysis of $NADP^+$, NADPH, NAD^+, NADH, reduced and oxidized glutathione, and with NH_3-saturated phenol/chloroform 1:1 for analysis of citrate and oxoglutarate. A Quattro Premier mass spectrometer interfaced with an Acquity UPLC system (Waters) was used for liquid chromatography-tandem mass spectrometry analysis. Calibration curves were established using standards, processed under the same conditions as the samples, at five concentrations. The best fit was determined using regression analysis of the peak analyte area. The multiple reaction monitoring transitions selected in the negative ion mode were *m/z* 190.95 > 110.89 for citrate and *m/z* 144.91 > 100.97 for oxoglutarate; multiple reaction monitoring transitions in the positive ion mode were *m/z* 744.06 > 507.83 for $NADP^+$, *m/z* 746.02 > 729.00 for NADPH, *m/z* 664.01 > 428.18 for NAD^+, *m/z* 666.19 > 649.10 for NADH, *m/z* 308.28 > 179.00 for GSH, and *m/z* 613.20 > 484.16 for GSSG. Chromatographic resolution was achieved using HSS T3 (2.1 $\times$

100 mm, 1.8-μm particle size, Waters) for citrate and oxoglutarate; Atlantis dC18 (4.6 × 150 mm, 5 μm particle size, Waters) for pyrimidine coenzymes; and BEH C18 (2.1 × 50 mm, 1.7 μm particle size, Interchim) for reduced and oxidized glutathione. For all columns, the flow rate was 0.3 ml/min.

ROS Measurements—ROS were assessed using 2′,7′-dichlorodihydrofluorescein diacetate (DCFH-DA) (17, 18). Fifteen micromolar DCFH-DA was added to cells in acetate-supplemented SC at the early exponential phase; after 30 min, the cells were washed once. For flow cytometric analysis, DCFH-DA-preloaded cells were incubated in the presence and absence of H_2O_2 (1 μmol × 10^7 cells) for the indicated times at 30 °C; DCF fluorescence was measured using a Coulter Epics Elite ESP (Beckman-Coulter) equipped with a 15-milliwatt argon-ion laser (excitation wavelength, 488 nm; emission wavelength, 520 nm) (19). For microplate reader assay, DCFH-DA-preloaded cells were incubated in the presence and absence of H_2O_2 (0.1 μmol × 10^5 cells) for the indicated times at 30 °C; DCF fluorescence was measured at 485-nm excitation and 538-nm emission wavelength (20).

Other Methods—Proteins were separated by SDS-PAGE and either stained with Coomassie Blue dye or transferred to nitrocellulose membranes. Matrix-assisted laser desorption ionization-time of flight (MALDI-TOF) mass spectrometry of trypsin digests of the purified Yhm2p band excised from a Coomassie-stained gel was carried out as described (21). Western blotting was carried out with rabbit antiserum against the bacterially expressed Yhm2p protein. The amount of purified protein was estimated by laser densitometry of stained samples using carbonic anhydrase as a protein standard (22). The amount of protein incorporated into liposomes was measured as described (22) and was ~20% of the protein added to the reconstitution mixture. To quantify the percentage of nonviable cells, wild-type and deleted strains in acetate-supplemented SC at the early exponential phase were exposed to H_2O_2 (1 μmol × 10^7 cells) for 1 h at 30 °C. Then they were washed in 15 mM $MgCl_2$ and 50 mM Tris-HCl, pH 7.7, resuspended in the same buffer containing 0.046 mM propidium iodide, and analyzed with a Coulter Epics Elite ESP (Beckman-Coulter) (23).

RESULTS

Expression in S. cerevisiae and Purification of Yhm2p—Yhm2p was expressed in *S. cerevisiae* from the multicopy *pYES2* vector and purified by nickel-nitrilotriacetic acid-agarose chromatography (supplemental Fig. S1). Its apparent molecular mass was about 34 kDa (supplemental Fig. S1*A, lane 4*), in agreement with the calculated value with the initiator methionine and histidine tag (34,985 Da). The identity of purified Yhm2p was confirmed by MALDI-TOF mass spectrometry. Approximately 70 mg of Yhm2p per liter of culture was obtained. The successful overexpression and targeting of episomal Yhm2p to mitochondria were confirmed by Western blotting. Thus, a strong immunoreactive band was detected in mitochondria isolated from *YHM2-pYES2* cells (supplemental Fig. S1*B, lane 3*) and a faint band in mitochondria from wild-type cells (supplemental Fig. S1*B, lane 1*), and no reaction was observed in mitochondria from the Δ*YHM2* mutant (supplemental Fig. S1*B, lane 2*).

Functional Characterization of Recombinant Yhm2p—In the search for potential substrates of Yhm2p, we based our choice on the fact that this protein displays residues at the proposed common substrate-binding site of MCs (24) that are nearly identical to those of the rat CTP and its yeast ortholog Ctp1p, which are known to transport citrate in exchange for malate (25–28). Thus, the substrate binding points are as follows: Gly^{93}–Lys^{97}–Arg^{101} (point I), Lys^{190}–Gln^{191} (point II), and Arg^{285} (point III) for CTP; Gly^{79}–Lys^{83}–Arg^{87} (point I), Arg^{181}–Gln^{182} (point II), and Arg^{279} (point III) for Ctp1p, which correspond to Glu^{83}–Lys^{87}–Leu^{91} (point I), Arg^{181}–Gln^{182} (point II), and Arg^{279} (point III) in Yhm2p. Therefore, recombinant and purified Yhm2p was reconstituted into liposomes, and its ability to transport citrate was tested. Indeed, proteoliposomes reconstituted with Yhm2p catalyzed active [^{14}C]citrate/citrate exchange, which was abolished by a mixture of the inhibitors pyridoxal 5′-phosphate and bathophenanthroline. They did not catalyze homo-exchanges for phosphate, aspartate, glutamate, ornithine, ADP, ATP, and GTP (internal concentration, 10 mM; external concentration, 1 mM). Furthermore, no [^{14}C]citrate/citrate exchange activity was detected if recombinant Yhm2p had been boiled before incorporation into liposomes.

The substrate specificity of purified and reconstituted Yhm2p was investigated in detail by measuring the uptake of [^{14}C]citrate into proteoliposomes that had been preloaded with various potential substrates (Fig. 1*A*). The highest rates of [^{14}C]citrate uptake into proteoliposomes were found with internal citrate, oxoglutarate, oxaloacetate, succinate, and fumarate. Surprisingly, at variance with the known mitochondrial citrate/malate carrier (25–28), reconstituted Yhm2p transported isocitrate, *cis*-aconitate, and L-malate with very low efficiency; it transported *trans*-aconitate at the same rate as *cis*-aconitate but did not transport 1,2,3-pentanetricarboxylate, maleate, and malonate. Yhm2p did also not catalyze uptake of [^{14}C]citrate in exchange for internal glutamate, oxoadipate, aspartate, phosphate, sulfate, and pyruvate and not shown ADP, ATP, GTP, thiosulfate, ornithine, glutamine, and carnitine.

The sensitivity of the Yhm2p-mediated [^{14}C]citrate/citrate exchange reaction by known inhibitors of different MCs was also examined. Thiol reagents (mersalyl, *p*-chloromercuribenzenesulfonate, mercuric chloride, and *N*-ethylmaleimide), the lysine reagent pyridoxal 5′-phosphate as well as bathophenanthroline and tannic acid (whose mechanism of action is not known) strongly inhibited citrate exchange; α-cyanocinnamate and bromcresol purple (whose mechanism of action is also unknown) inhibited citrate exchange partially (Fig. 1*B*). In contrast, 1,2,3-benzenetricarboxylate and carboxyatractyloside, the powerful inhibitors of the citrate/malate carrier (27) and the ADP/ATP carrier (29), respectively, had very little effect on the activity of Yhm2p. The competitive inhibitors of the dicarboxylate and oxoglutarate/malate carriers, butylmalonate and phenylsuccinate, were also rather ineffective. In addition, externally added citrate, oxoglutarate, succinate, and fumarate inhibited the [^{14}C]citrate/citrate exchange (Fig. 1*B*). A low inhibition was found with malate and virtually no effect was detected with glutamate and ATP.

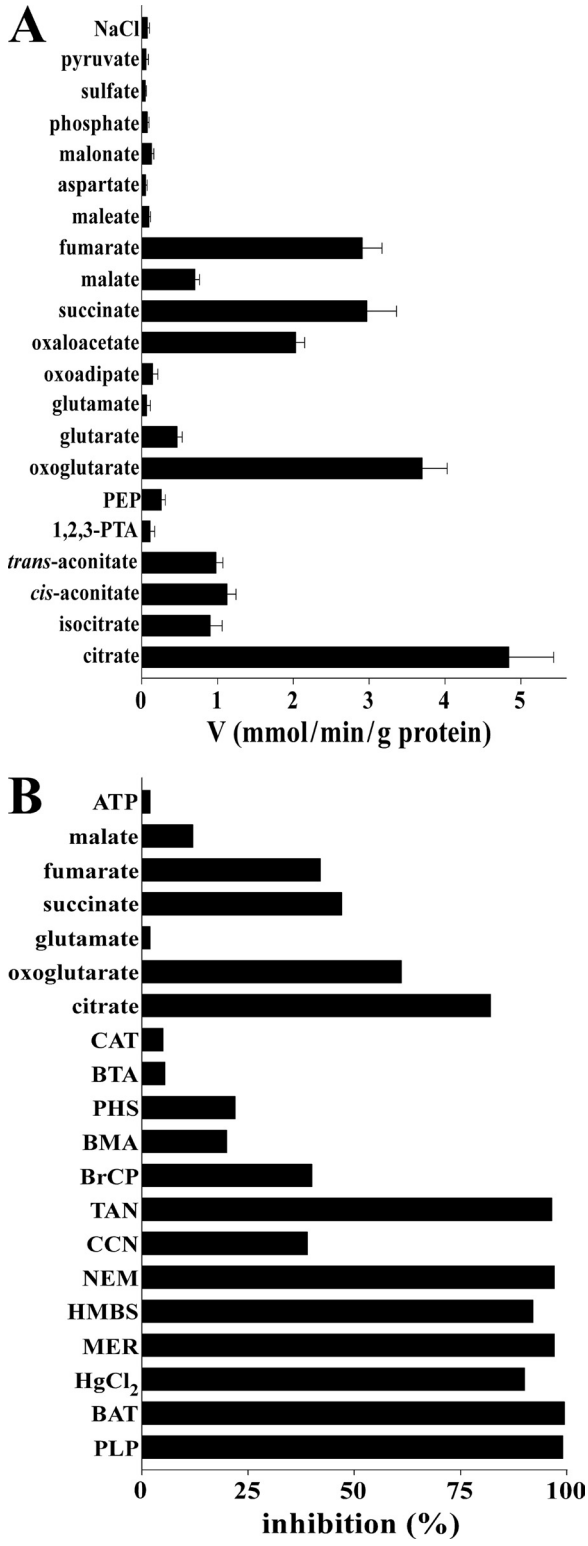

FIGURE 1. **Substrate specificity of recombinant and reconstituted Yhm2p.** *A,* dependence of Yhm2p activity on internal substrate. Proteoliposomes were preloaded internally with various substrates (concentration, 20 mM). Transport was initiated by adding 0.15 mM [^{14}C]citrate to proteoliposomes and terminated after 1 min. Values are means ± S.E. of at least three independent experiments. Abbreviations used are as follows: *1,2,3-PTA*, 1,2,3-pentanetricarboxylate; *PEP*, phosphoenolpyruvate. *B,* effect of inhibitors and external substrates on the [^{14}C]citrate/citrate exchange catalyzed by reconstituted Yhm2p. Proteoliposomes were preloaded internally with 20 mM citrate, and transport was initiated by adding 0.15 mM [^{14}C]citrate. The incubation time was 1 min. Thiol reagents and α-cyanocinnamate were added 2 min before the labeled substrate; the other indicated inhibitors and substrates were added together with [^{14}C]citrate. The final concentrations of the inhibitors were 0.1 mM (*HMBS*, *p*-hydroxymercuribenzene sulfonate; *$HgCl_2$*, mercuric chloride; *MER*, mersalyl), 10 mM (*PLP*, pyridoxal 5′-phosphate; *BAT*, bathophenanthroline), 1 mM (*NEM*, *N*-ethylmaleimide; *CCN*, α-cyanocinnamate), 2 mM (*BTA*, benzene 1,2,3-tricarboxylate; *BMA*, butylmalonate; *PHS*, phenylsuccinate), 0.2 mM (*BrCP*, bromcresol purple), 0.05% (*TAN*, tannic acid), and 10 μM (*CAT,* carboxyatractyloside). The final concentration of unlabeled substrates added together with [^{14}C]citrate was 3 mM. The extents of inhibition (%) from a representative experiment are given. Similar results were obtained in at least three independent experiments.

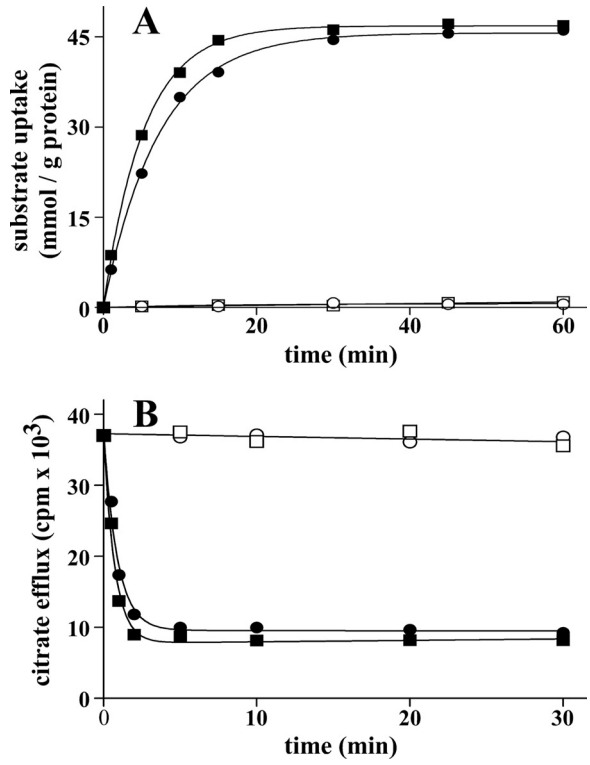

FIGURE 2. **Kinetics of [^{14}C]citrate and [^{14}C]oxoglutarate transport in proteoliposomes reconstituted with Yhm2p.** *A,* uptake of citrate or oxoglutarate. 2 mM [^{14}C]citrate or [^{14}C]oxoglutarate was added to proteoliposomes containing 20 mM citrate (■) or oxoglutarate (●), respectively (exchange), or 10 mM NaCl and no substrate for either citrate (□) or oxoglutarate (○) uptake (uniport). *B,* efflux of [^{14}C]citrate from proteoliposomes reconstituted in the presence of 1 mM citrate. The internal substrate pool was labeled with [^{14}C]citrate by carrier-mediated exchange equilibration. Then the proteoliposomes were passed through Sephadex G-75. The efflux of [^{14}C]citrate was started by adding buffer G alone (□), 5 mM citrate (■), or oxoglutarate (●) in buffer G or 5 mM citrate, 30 mM pyridoxal 5′-phosphate, and 10 mM bathophenanthroline in buffer G (○). Similar results were obtained in three independent experiments for both uptake and efflux.

Kinetic Characteristics of Recombinant Yhm2p—The time courses of [^{14}C]citrate and [^{14}C]oxoglutarate uptake into proteoliposomes were measured either as uniport (in the absence of internal substrate) or as antiport (in the presence of internal citrate or oxoglutarate, respectively) (Fig. 2*A*). The uptake of citrate or oxoglutarate by exchange followed a first order kinetics (rate constants, 0.18 and 0.13 min^{-1}; initial rates, 8.84 and 6.29 mmol/min/g of protein for citrate and oxoglutarate, respectively), isotopic equilibrium being approached exponentially. In contrast, the uniport uptake of citrate and oxoglutarate was negligible, suggesting that Yhm2p does not catalyze a unidirectional transport (uniport) of citrate or oxoglutarate. This issue was further investigated by measuring the efflux of

[^{14}C]citrate from prelabeled active proteoliposomes, as this provides a more sensitive assay for unidirectional transport (12). In the absence of external substrate, no efflux was observed even after a 30-min incubation (Fig. 2*B*). However, addition of external citrate or oxoglutarate led to extensive efflux of radioactivity, which was prevented completely by the presence of the inhibitors pyridoxal 5′-phosphate and bathophenanthroline (Fig. 2*B*). These results demonstrate that, at least under the experimental conditions employed, reconstituted Yhm2p catalyzes an obligatory antiport reaction of substrates.

The kinetic constants of purified reconstituted Yhm2p were determined by measuring the initial transport rate at various external [^{14}C]citrate or [^{14}C]oxoglutarate concentrations in the presence of a constant saturating internal concentration of either citrate or oxoglutarate. With both citrate- and oxoglutarate-loaded proteoliposomes, linear functions were obtained in double-reciprocal plots. These were independent of the internal substrate and intersected the ordinate close to a common point. The average V_{max} values of citrate and oxoglutarate uptake (9.8 ± 1.2 mmol/min per g of protein for the [^{14}C]citrate/citrate and [^{14}C]citrate/oxoglutarate exchanges and 10.3 ± 2.1 mmol/min per g of protein for the [^{14}C]oxoglutarate/oxoglutarate and [^{14}C]oxoglutarate/citrate exchanges) were virtually the same. The half-saturation constant (K_m) for citrate was 0.16 ± 0.05 mM and that for oxoglutarate was 1.2 ± 0.15 mM. Oxoglutarate inhibited [^{14}C]citrate/citrate exchange competitively as did succinate, oxaloacetate, fumarate, and malate. The inhibition constants (K_i) of these substrates for Yhm2p were the following: 1.2 ± 0.12 mM (oxoglutarate), 1.46 ± 0.08 mM (succinate), 1.73 ± 0.18 mM (oxaloacetate), 1.87 ± 0.21 mM (fumarate), and 6.2 ± 0.7 mM (malate) in four experiments for each inhibitor.

Impaired Citrate Uptake in Mitochondria Lacking Yhm2p—In other experiments, the uptake of [^{14}C]citrate was measured in proteoliposomes that had been reconstituted with Triton X-100 extracts of mitochondria isolated from wild-type, Δ*YHM2*, and *YHM2-pYES2* cells (Fig. 3). A low citrate/citrate exchange activity was observed upon reconstitution of mitochondrial extracts from the knock-out strain, probably because of the presence of Ctp1p. This activity more than doubled in parental mitochondrial extracts and was even greater in mitochondrial extracts from *YHM2-pYES2* cells. Similar results were obtained by measuring the uptake of [^{14}C]citrate in exchange with intraliposomal oxoglutarate, succinate, fumarate, and oxaloacetate (Fig. 3), which are substrates of Yhm2p, but not with substrates of other MCs such as phosphate, ADP, maleate, 1,2,3-pentanetricarboxylate, glutamate, carnitine, and ornithine. Moreover, the citrate/citrate exchange in proteoliposomes reconstituted with mitochondrial extracts from wild-type and *YHM2-pYES2* cells was markedly inhibited by mercurials, *N*-ethylmaleimide and tannic acid (data not shown). As a control, the [^{14}C]ADP/ATP exchange (the defining reaction of the ADP/ATP translocase) and the [^{14}C]malate/phosphate exchange (the defining reaction of the dicarboxylate carrier) were virtually the same for all types of reconstituted mitochondrial extracts (data not shown). Moreover, as demonstrated by immunodecorating wild-type and Δ*YHM2* mitochondria with

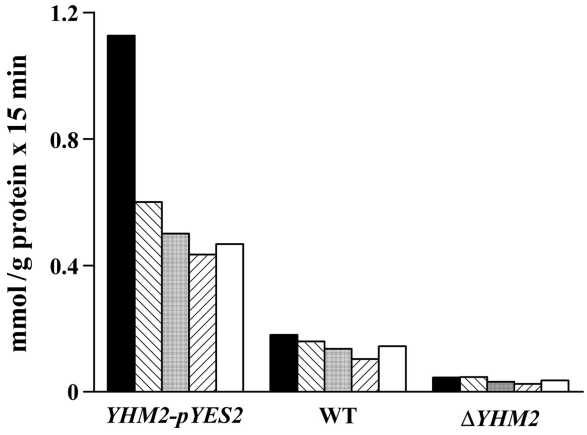

FIGURE 3. **Citrate exchange activities in liposomes reconstituted with mitochondrial extracts from the Δ*YHM2* strain, parental strain, and the parental strain transformed with the *YHM2-pYES2* plasmid.** These strains were grown as indicated under "Experimental Procedures" for *YHM2-pYES2* cells. Mitochondria were isolated and solubilized with 1% Triton X-100, 50 mM NaCl, and 10 mM PIPES, pH 7.0. The extracts (30 μg of protein) were reconstituted into liposomes preloaded with 20 mM citrate (*black columns*), oxoglutarate (*hatched columns*), succinate (*gray columns*), oxaloacetate (*inverted hatched columns*), or fumarate (*white columns*). Transport was started by adding 0.15 mM [^{14}C]citrate and terminated after 15 min. *WT*, wild type.

specific antibodies, the amounts of the ADP/ATP, phosphate, and dicarboxylate carriers were virtually the same (results not shown). Therefore, in mitochondria Yhm2p exhibits the same specificity and inhibitor sensitivity as the purified protein; moreover, the absence of *YHM2* does not affect the expression or the activity of other MCs.

Subcellular Localization of Yhm2p—Yhm2p has been reported to be localized to the inner mitochondrial membrane (1). However, these studies did not exclude the possibility that Yhm2p is also localized to peroxisomes, notably because its transport properties make it a candidate for being involved in a peroxisomal redox shuttle that is required for the intraperoxisomal regeneration of NADPH (30, 31). Also, Yhm2p was among the proteins that had been identified in a purified peroxisomal membrane fraction by mass spectrometry (32). The subcellular distribution of Yhm2p was therefore analyzed by separating a post-nuclear supernatant of oleic acid-induced wild-type cells on a sucrose density gradient. The enzyme activities of the mitochondrial marker enzyme fumarase and peroxisomal enzyme catalase were separated with some overlapping in fractions 13–17 (supplemental Fig. S2*A*). The immunoblots of fractions 3–29 demonstrate co-localization of Yhm2p with the mitochondrial phosphate transporter Mir1p and no co-localization of Yhm2p with Fox3p, although overlapping was observed in fraction 15 (supplemental Fig. S2*A*). To obtain further proof of the localization of Yhm2p, BJ1991*pox1*Δ, the strain used for the mass spectrometric analysis of peroxisomal membrane proteins (32), was induced in the presence of oleic acid. A post-nuclear supernatant was separated on a sucrose gradient, and the fractions enriched for peroxisomes were pooled, concentrated, and further separated on an Accudenz gradient. The subsequent immunological analysis using anti-Fox3p and anti-Pex11p antibodies showed peroxisomes peaking in fractions 8 and 9, whereas mitochondrial Mir1p peaked in fractions 12–15 (supplemental Fig. S2*B*) demonstrating the successful separation of peroxisomes from mitochondria. The

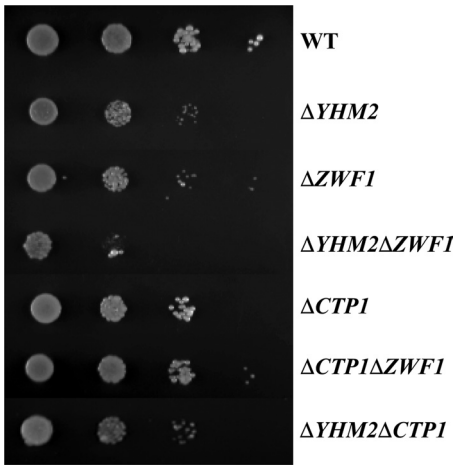

FIGURE 4. **Growth behavior of Δ*YHM2*, Δ*ZWF1*, Δ*YHM2*Δ*ZWF1*, Δ*CTP1*, Δ*CTP1*Δ*ZWF1*, and Δ*YHM2*Δ*CTP1* strains in acetate-supplemented SM.** 4-Fold serial dilutions of equally numbered wild-type (*WT*), Δ*YHM2*, Δ*ZWF1*, Δ*YHM2*Δ*ZWF1*, Δ*CTP1*, Δ*CTP1*Δ*ZWF1*, and Δ*YHM2*Δ*CTP1* cells (precultured overnight in YP with glucose) were plated on solid acetate-supplemented SM at 30 °C.

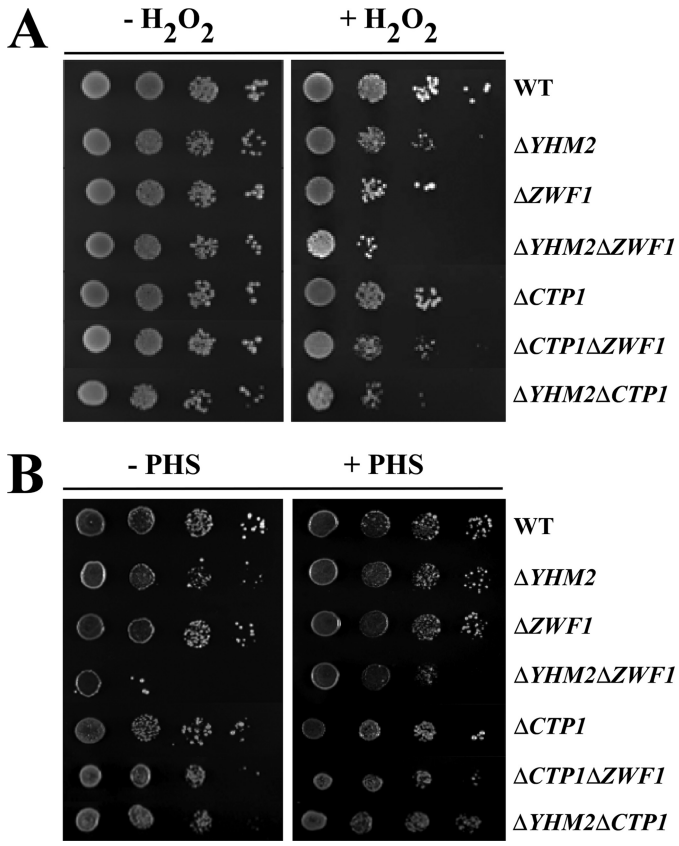

FIGURE 5. **Growth behavior of Δ*YHM2*, Δ*ZWF1*, Δ*YHM2*Δ*ZWF1*, Δ*CTP1*, Δ*CTP1*Δ*ZWF1*, and Δ*YHM2*Δ*CTP1* strains in acetate-supplemented SC in the presence or absence of H_2O_2 (*A*) and phytosphingosine (*B*).** 4-Fold serial dilutions of equally numbered wild-type (*WT*), Δ*YHM2*, Δ*ZWF1*, Δ*YHM2*Δ*ZWF1*, Δ*CTP1*, Δ*CTP1*Δ*ZWF1*, and Δ*YHM2*Δ*CTP1* cells (precultured overnight in YP with glucose) were plated on solid acetate-supplemented SC with or without 1.25 mM H_2O_2 at 30 °C (*A*) and 5 μM phytosphingosine (*PHS*) at 37 °C (*B*).

Yhm2p-specific signal co-migrated with that of Mir1p, and no additional peroxisomal peak was detectable (supplemental Fig. S2*B*).

Localization of Yhm2p was also investigated in live cells by expressing a Yhm2p-GFP fusion protein from the native *YHM2* promoter. Co-expression of a synthetic mitochondrial inner membrane marker protein (PrF_0ATP9) that had been fused with DsRed (33) resulted in an overlapping pattern of fluorescence for the two proteins (data not shown). Contrarily, co-expression of a peroxisomally targeted PTS2-DsRed construct (33), displaying the typical punctate peroxisomal staining pattern, revealed that Yhm2p-GFP-dependent fluorescence did not coincide with peroxisomes (data not shown). These data demonstrate that Yhm2p is not a peroxisomal protein, in contrast to a previous conclusion (32), but is a mitochondrial protein in agreement with Cho *et al.* (1).

Growth Phenotypes of Knock-out Yeast Strains and Mitochondrial Citrate Levels—Having established the transport properties of Yhm2p by *in vitro* assays and its mitochondrial localization, the physiological role of Yhm2p was investigated. We first tested the ability of the Δ*YHM2* strain to grow under various conditions. Yeast cells lacking *YHM2* exhibited substantial growth on YP and SC media containing either fermentative or nonfermentative carbon sources, similarly to the wild-type strain. However, on acetate-supplemented SM, Δ*YHM2* cells exhibited a slightly greater growth defect than that of Δ*ZWF1* cells (Fig. 4). The double mutant Δ*YHM2*Δ*ZWF1* exhibited a more pronounced defect than the single mutants when compared with wild-type cells. The growth of Δ*CTP1*, Δ*CTP1*Δ*ZWF1*, and Δ*YHM2*Δ*CTP1* cells was less affected (Fig. 4). On acetate-supplemented SC, in the presence of amino acids, none of the investigated strains showed any defect (Fig. 5*A*). However, when treated with H_2O_2, Δ*YHM2* cells exhibited a growth defect that was more evident in the double mutant Δ*YHM2*Δ*ZWF1* (Fig. 5*A*). Also, in the presence of H_2O_2, the Δ*CTP1* strain exhibited a lesser growth defect than the Δ*YHM2* strain as evidenced by the second and third dilutions of the two strains. Moreover, the Δ*CTP1*Δ*ZWF1* and Δ*YHM2*Δ*CTP1* double mutants were less sensitive to the H_2O_2-induced stress than the Δ*YHM2*Δ*ZWF1* double mutant; their growth defects were almost equal to those caused by the Δ*ZWF1* and Δ*YHM2* strains, respectively (Fig. 5*A*). We then investigated the effect of deleting *YHM2* on citrate content in the mitochondria of *S. cerevisiae* cells grown on acetate-supplemented SC. Δ*YHM2* cells showed a significant increase (by 77%) in the amount of intramitochondrial citrate (1.6 ± 0.2 nmol/mg of protein) as compared with wild-type cells (0.9 ± 0.2 nmol/mg of protein), suggesting that Yhm2p may function to catalyze export of citrate from mitochondria to cytosol. In the cytosol, citrate is converted to isocitrate, which is the substrate of isocitrate dehydrogenase (Idp2p) that produces oxoglutarate and reduces $NADP^+$ to NADPH. On this basis, the observed phenotypes could be due to diminished NADPH in the cytosol because this coenzyme is used to produce important antioxidants, such as GSH by glutathione reductase.

The first indication in support of this hypothesis stems from experiments carried out at 37 °C in the presence or absence of phytosphingosine. When cultured at ≥37 °C, yeast cells undergo major changes to increase thermotolerance and the ability to continue to divide. For example, at 37 °C they increase the synthesis of ceramides by means of a pathway that includes

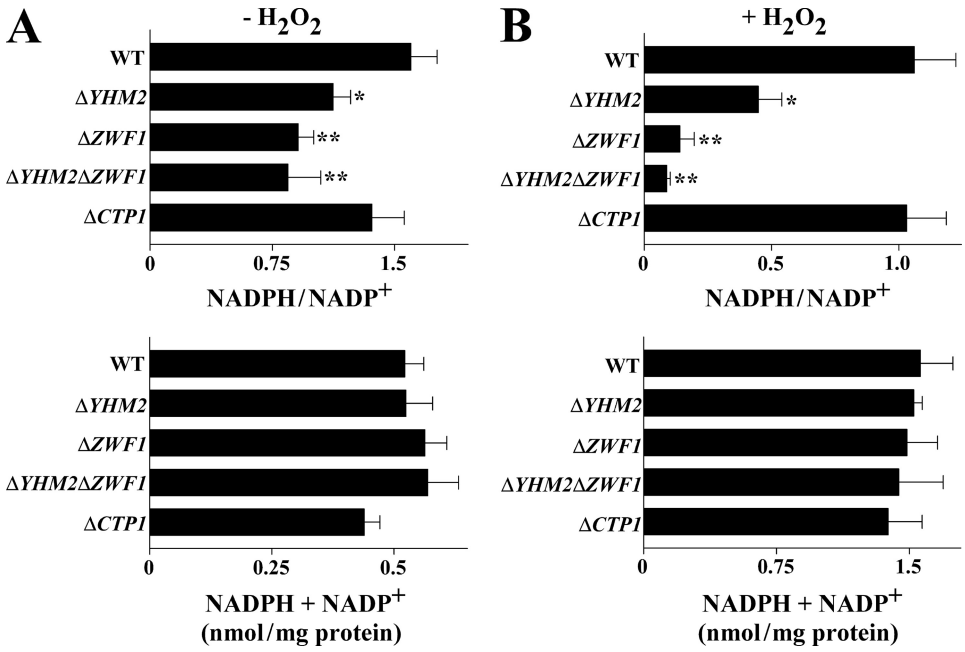

FIGURE 6. **NADPH/NADP$^+$ ratios in the cytosol of parental and deleted *S. cerevisiae* strains.** Yeast strains, precultured in YP with glucose and grown in acetate-supplemented SC, were incubated in the presence (*B*) or absence (*A*) of H_2O_2 for 60 min. NADPH/NADP$^+$ ratios and the sums of NADPH + NADP$^+$ are reported as means ± S.E. of at least three independent experiments. Differences between the NADPH/NADP$^+$ ratio of Δ*YHM2*, Δ*ZWF1*, and Δ*YHM2*Δ*ZWF1* cells and control (wild-type (*WT*) cells), with and without H_2O_2, were significant (*, $p < 0.05$, and **, $p < 0.01$, one-way ANOVA followed by Bonferroni's *t* test).

phytosphingosine as an intermediate (34, 35). Given that NADPH is required in the last two reactions of phytosphingosine biosynthesis catalyzed by Tsc10 and Sur2, respectively, we tested the ability of our strains to grow at 37 °C in acetate-supplemented SC. Δ*YHM2*Δ*ZWF1* cells were temperature-sensitive, and this phenotype was partially rescued by the addition of phytosphingosine (Fig. 5*B*). The deletant Δ*YHM2* also exhibited a slight growth defect at 37 °C as evidenced by comparing the third and fourth dilutions between wild-type and Δ*YHM2* cells; this defect was also prevented by phytosphingosine (Fig. 5*B*). The double knock-out Δ*YHM2*Δ*CTP1* exhibited a temperature sensitivity almost equal to that of the Δ*YHM2* strain but not greater.

Cytosolic Levels of Nicotinamide Coenzymes and Glutathione—In light of the phenotypes exhibited by the knock-out strains for *YHM2* and *ZWF1* upon exposure to H_2O_2 or at 37 °C, the levels of cytosolic NADPH and NADP$^+$ were measured. Without H_2O_2 treatment, the cytosolic NADPH/NADP$^+$ ratio in the Δ*YHM2* strain was significantly lower than that measured in the wild-type strain (Fig. 6*A*). This ratio decreased further (by about 43 and 48%) in the Δ*ZWF1* and Δ*YHM2*Δ*ZWF1* strains; however, it was not decreased in Δ*CTP1* cells as compared with wild-type cells. Moreover, no significant variations in the total amount of NADP$^+$ plus NADPH were observed among the different strains (Fig. 6*A*). After treatment with H_2O_2, the NADPH/NADP$^+$ ratio was significantly decreased in the Δ*YHM2* strain (by 58%), more in the Δ*ZWF1* strain (by 87%) and further still in the double knock-out strain (by 91%) as compared with the wild-type strain (Fig. 6*B*). Again, the NADPH/NADP$^+$ ratio was not decreased in Δ*CTP1* cells. Moreover, the changes in this ratio observed in H_2O_2-treated Δ*YHM2*, Δ*ZWF1*, and Δ*YHM2*Δ*ZWF1* cells were not accompanied by variations in the total amount of NADP$^+$ plus NADPH (Fig. 6*B*). Of note, the total amount of NADP(H) was about three times higher in the presence of H_2O_2 than in its absence, likely due to the activity of cytosolic Utr1p and Yef1p, which phosphorylate NADH to NADPH. In addition, it is worthwhile mentioning that the NADPH/NADP$^+$ ratio was decreased in the double mutant Δ*YHM2*Δ*CTP1*, with and without H_2O_2, to an extent similar to that observed in the single mutant Δ*YHM2* (data not shown). These results indicate that the reduction of the NADPH/NADP$^+$ ratio is caused by the absence of *YHM2*, and not of *CTP1*. In the next step, the cytosolic levels of NADH and NAD$^+$ were measured. In the absence of H_2O_2, no significant changes in either the NADH/NAD$^+$ ratio or in the total amount of NAD$^+$ plus NADH were observed among the different strains (supplemental Fig. S3*A*). After treatment with H_2O_2, the NADH/NAD$^+$ ratio (but not the total amount of NAD$^+$ plus NADH) decreased in the Δ*YHM2*, Δ*ZWF1*, and Δ*YHM2*Δ*ZWF1* strains (supplemental Fig. S3*B*), although to a lesser extent than the NADPH/NADP$^+$ ratio, as compared with wild type. Moreover, the total amount of NADH + NAD$^+$ was increased in the presence of H_2O_2. The NADH/NAD$^+$ ratio was also not affected by H_2O_2 in the Δ*CTP1* strain as compared with wild type (supplemental Fig. S3*B*).

Given that NADPH can be oxidized by glutathione reductase, reduced and oxidized glutathione levels in the cytosol were measured. In the absence of H_2O_2, the GSH/GSSG ratio was reduced in Δ*YHM2* (by 43%), Δ*ZWF1* (by 55%), and in Δ*YHM2*Δ*ZWF1* (by 60%) strains but not in Δ*CTP1* cells as compared with wild type (Fig. 7*A*). In contrast, the total amount of glutathione did not show significant changes among strains. In the presence of H_2O_2, the GSH/GSSG ratio was reduced by 35% in Δ*YHM2* cells as compared with wild type without variation in the total amount of glutathione (Fig. 7*B*). In Δ*ZWF1* cells, the ratio was markedly decreased (by 85%) along with a decrease in total glutathione (by 52%), probably because part of GSH was used to protect proteins from oxidative damage by derivatizing key thiol groups. As compared with Δ*ZWF1* cells, Δ*YHM2*Δ*ZWF1* cells exhibited a smaller reduction of the GSH/GSSG ratio (by 72%) together with a smaller decrease in total glutathione (by 30%) with respect to wild-type cells. This finding may be due to the severe stress condition caused by adding H_2O_2 to the double knock-out, which led to *ex novo* synthesis of GSH besides protein glutathionylation. In fact, the total amount of glutathione in all the strains was greatly increased in

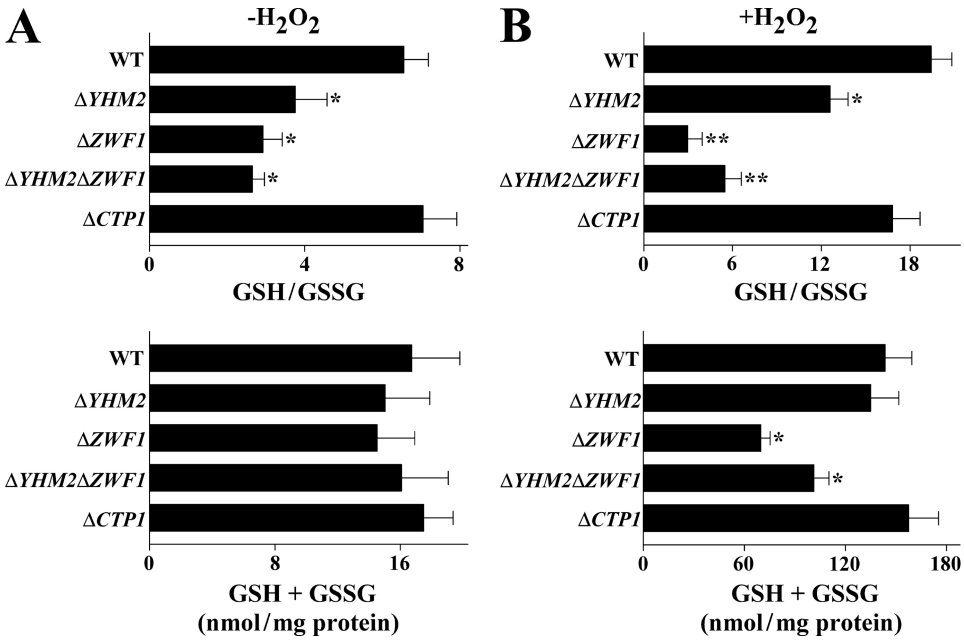

FIGURE 7. **GSH/GSSG ratios in the cytosol of parental and deleted *S. cerevisiae* strains.** Yeast strains, precultured in YP with glucose and grown in acetate-supplemented SC, were incubated in the presence (*B*) or absence (*A*) of H_2O_2 for 60 min. GSH/GSSG ratios and the sums of GSH + GSSG are reported as means ± S.E. of at least three independent experiments. Differences between the GSH/GSSG ratio of Δ*YHM2*, Δ*ZWF1*, and Δ*YHM2*Δ*ZWF1* cells and control (wild-type (*WT*) cells), with and without H_2O_2, were significant (*, $p < 0.05$, and **, $p < 0.01$, one-way ANOVA followed by Bonferroni's *t* test). Differences between the sum of GSH + GSSG of Δ*ZWF1* and Δ*YHM2*Δ*ZWF1* and control (wild-type cells) in the presence of H_2O_2 were significant (*, $p < 0.05$, one-way ANOVA followed by Bonferroni's *t* test).

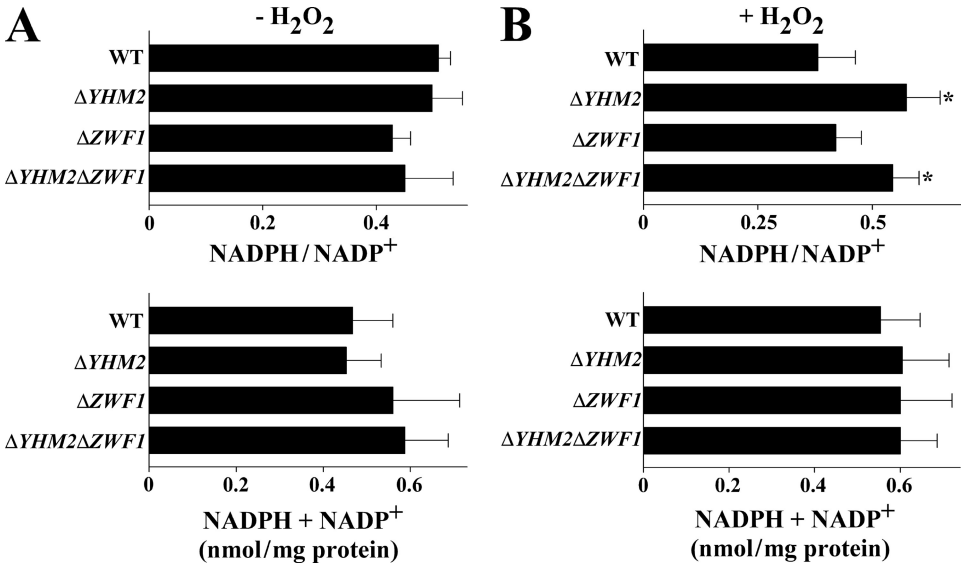

FIGURE 8. **NADPH/NADP$^+$ ratios in the mitochondria of parental and deleted *S. cerevisiae* strains.** Yeast strains, precultured in YP with glucose and grown in acetate-supplemented SC, were incubated in the presence (*B*) or absence (*A*) of H_2O_2 for 60 min. NADPH/NADP$^+$ ratios and the sums of NADPH + NADP$^+$ are reported as means ± S.E. of at least three independent experiments. Differences between the NADPH/NADP$^+$ ratio of Δ*YHM2* and Δ*YHM2*Δ*ZWF1* cells and control (wild-type (*WT*) cells) in the presence of H_2O_2 were significant (*, $p < 0.05$, one-way ANOVA followed by Bonferroni's *t* test).

the presence of H_2O_2 as compared with its absence. Again, the ratio between GSH and GSSG was not significantly decreased in Δ*CTP1* cells (Fig. 7*B*).

Nicotinamide Coenzyme Levels in Mitochondria—Once ascertained that deletion of *YHM2*, *ZWF1*, or both decreases the cytosolic NADPH/NADP$^+$ ratio, especially upon H_2O_2 treatment, this ratio was determined in the mitochondria of knock-out strains. With no addition of H_2O_2, the mitochondrial NADPH/NADP$^+$ ratio was approximately the same in all the evaluated strains (Fig. 8*A*). However, upon addition of H_2O_2, this ratio was significantly higher in Δ*YHM2* and Δ*YHM2*Δ*ZWF1* strains as compared with the wild-type strain (Fig. 8*B*). In all strains, the total amount of NADPH and NADP$^+$ coenzymes was similar regardless of H_2O_2 treatment. Therefore, under oxidative stress, the NADPH/NADP$^+$ ratio of Δ*YHM2* and Δ*YHM2*Δ*ZWF1* cells diminished in the cytosol (Fig. 6*B*) and increased in mitochondria (Fig. 8*B*), suggesting that in wild-type cells reducing equivalents of NADPH can be transferred from the mitochondria to the cytosol through the activity of Yhm2p. In untreated wild-type and knock-out cell mitochondria, the NADH level was too low, as observed previously in wild-type cells (15), to assess the NADH/NAD$^+$ ratio. Upon addition of H_2O_2, both the low NADH/NAD$^+$ ratio and total amount of NADH + NAD$^+$ were not significantly different among the strains tested (supplemental Fig. S4*B*).

Cytosolic Citrate and Oxoglutarate Levels—Cytosolic samples of Δ*YHM2*, Δ*ZWF1*, and Δ*YHM2*Δ*ZWF1* cells were also analyzed for the two exchanging metabolites citrate and oxoglutarate. Of note, the cytosol of H_2O_2-treated wild-type cells contained much more citrate than the cytosol of untreated cells (217 nmol/mg protein as compared with 37 nmol/mg protein without H_2O_2; Fig. 9, *A* and *B*), presumably due to the activity of the extra-mitochondrial citrate-producing enzyme Cit2p. Moreover, the cytosol of H_2O_2-treated Δ*YHM2*, Δ*ZWF1*, and Δ*YHM2*Δ*ZWF1* cells contained a significantly lower amount of citrate (by about 27%) than the same fraction of wild-type cells (Fig. 9*B*). On the contrary, with no treatment the cytosolic level of citrate was approximately the same in the deleted strains as the in wild-type cells (Fig. 9*A*). Concerning oxoglutarate, without H_2O_2 treatment, its level in the cytosol was similar in Δ*ZWF1*, higher in Δ*YHM2*, and significantly higher in Δ*YHM2*Δ*ZWF1* cells as compared with wild-type cells

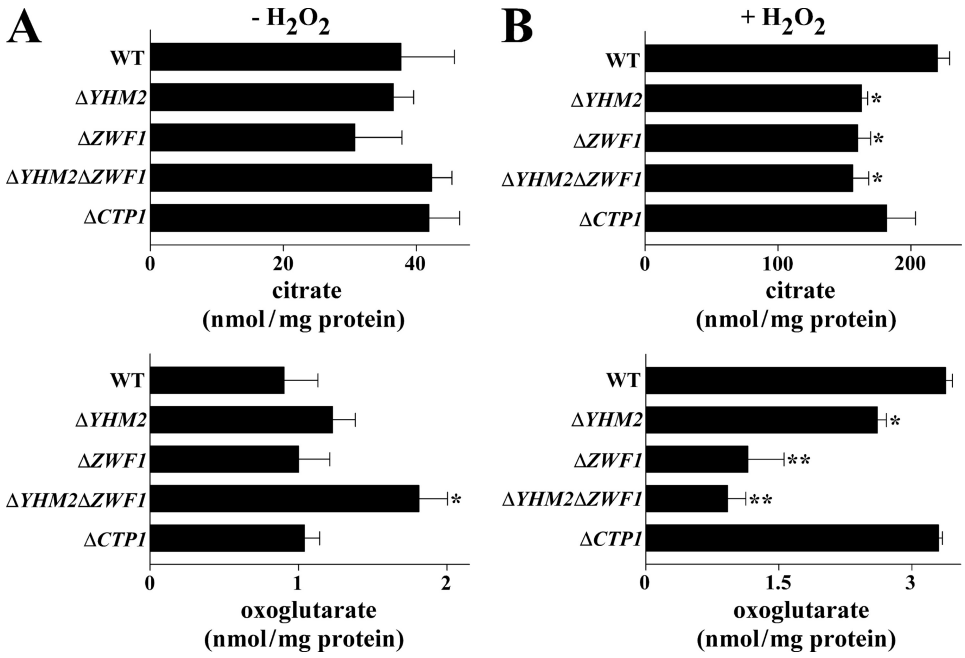

FIGURE 9. **Citrate and oxoglutarate levels in the cytosol of parental and deleted *S. cerevisiae* strains.** Yeast strains, precultured in YP with glucose and grown in acetate-supplemented SC, were incubated in the presence (*B*) or absence (*A*) of H_2O_2 for 60 min. Means ± S.E. of at least three independent experiments are reported. Differences between cytosolic citrate of Δ*YHM2*, Δ*ZWF1*, and Δ*YHM2*Δ*ZWF1* cells and control (wild-type (*WT*) cells) in the presence of H_2O_2 were significant (*, $p < 0.05$, one-way ANOVA followed by Bonferroni's *t* test). The difference between cytosolic oxoglutarate of Δ*YHM2*Δ*ZWF1* and wild-type cells in the absence of H_2O_2 is significant (*, $p < 0.05$). Differences between cytosolic oxoglutarate of Δ*YHM2*, Δ*ZWF1*, and Δ*YHM2*Δ*ZWF1* cells and wild-type cells in the presence of H_2O_2 were significant (*, $p < 0.05$, and **, $p < 0.01$, one-way ANOVA followed by Bonferroni's *t* test).

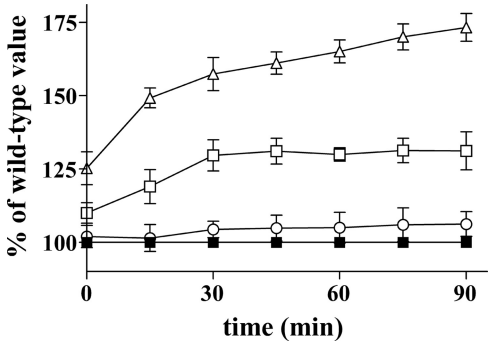

FIGURE 10. **Cell antioxidant response to oxidative stress.** DCFH-DA-preloaded wild-type (■), Δ*YHM2* (○), Δ*ZWF1* (□), and Δ*YHM2*Δ*ZWF1* (△) cells were incubated in acetate-supplemented SC in the presence of H_2O_2 for the indicated time periods. DCF fluorescence was measured using a microplate reader and expressed as the percentage of the corresponding wild-type values. Values are means ± S.E. of four independent experiments.

(Fig. 9*A*). By contrast, in the presence of H_2O_2 the cytosolic level of oxoglutarate was moderately (but significantly) reduced in Δ*YHM2* and more so in Δ*ZWF1* and Δ*YHM2*Δ*ZWF1* cells as compared with wild-type cells (Fig. 9*B*). This indicates that under these stress conditions oxoglutarate is most likely used to produce the antioxidant tripeptide GSH.

Antioxidant Response to H_2O_2 Exposure—The intracellular DCF fluorescence (*i.e.* level of intracellular non-scavengered ROS (18)) of Δ*YHM2* cells exposed to H_2O_2 was slightly higher than that of H_2O_2-treated wild-type cells (Fig. 10). In contrast, the fluorescence increased to 131 ± 7 and 173 ± 5% in the Δ*ZWF1* and Δ*YHM2*Δ*ZWF1* cells, respectively, after a 90-min H_2O_2 exposure compared with that of treated wild-type cells (Fig. 10). These findings indicate that the cells lacking both *YHM2* and *ZWF1* responded to oxidative insult much less efficiently than the individually deleted strains. The ROS scavenger ability of wild-type and deleted cells was further assessed by cytofluorimetry. The histograms of time-dependent fluorescence-activated cell sorter analysis (Fig. 11) show that the intensity of cell fluorescence was markedly increased after a 30-min H_2O_2 exposure for the Δ*YHM2*Δ*ZWF1* cells and after a 60-min H_2O_2 exposure also for the single deleted cells. Specifically, following a 60-min H_2O_2 incubation, 7, 64, 86, and 96% of wild-type, Δ*YHM2*, Δ*ZWF1*, and Δ*YHM2*Δ*ZWF1* cells, respectively, displayed high fluorescence intensity.

The effects of the H_2O_2 treatment used in the experiments described above on cell viability are reported in supplemental Table S2. After a 1-h incubation with H_2O_2, the percentage of nonviable cells increased to ~5.3% (from ~1.6% without H_2O_2) for the wild-type and single deleted cells and somewhat more (to 8.2%) for the Δ*YHM2*Δ*ZWF1* double mutant. By contrast, virtually all cells died when boiled.

DISCUSSION

In this work, overexpression in *S. cerevisiae* of a previously unidentified MC and reconstitution of the recombinant protein in liposomes as well as phenotype analysis of yeast knock-out cells have been employed to investigate the function of Yhm2p. The transport properties and kinetic parameters of Yhm2p, together with its mitochondrial localization, demonstrate that this protein is a novel mitochondrial citrate-oxoglutarate carrier. Besides transporting these substrates with great efficiency, Yhm2p also translocates oxaloacetate, fumarate, succinate, and to a much lesser extent, L-malate and other tricarboxylates.

The substrate specificity of Yhm2p is distinct from that of any other MC of known sequence and function, including the carriers for carboxylates, although Yhm2p is phylogenetically related to these proteins (6, 36, 37) and shares some degree of substrate overlap. In particular, Yhm2p differs markedly from the citrate/malate carrier (25–28) because this protein efficiently transports tricarboxylates (citrate, isocitrate, *cis*-aconitate, 1,2,3,-pentanetricarboxylate, but not *trans*-aconitate), dicarboxylates (malate, succinate, malonate, and maleate but not oxoglutarate, oxaloacetate, and fumarate), and phosphoenolpyruvate. Furthermore, Yhm2p is not inhibited by 1,2,3,-benzenetricarboxylate, a powerful inhibitor of the rat and yeast citrate/malate carriers (25–28), and is strongly sensitive to

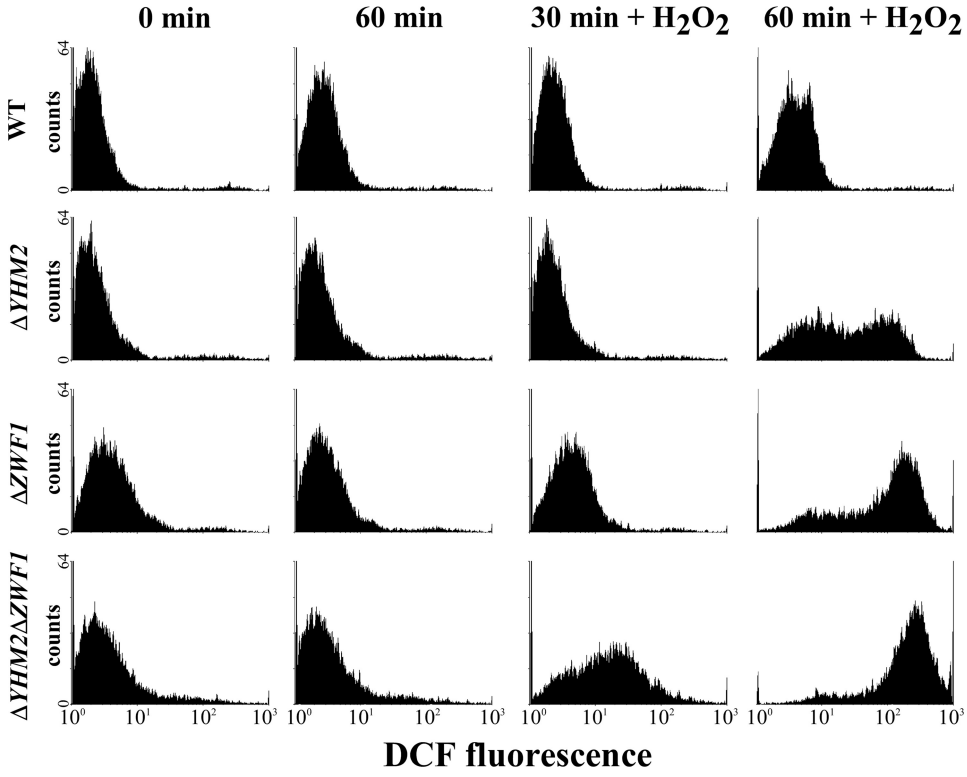

FIGURE 11. **Flow cytometric analysis of ROS levels in wild-type and knock-out *S. cerevisiae* strains.** DCFH-DA-preloaded wild-type (*WT*), Δ*YHM2*, Δ*ZWF1*, and Δ*YHM2*Δ*ZWF1* cells were incubated in acetate-supplemented SC in the presence or absence of H_2O_2 for the time periods indicated. Results from a representative experiment are shown as cell number (counts) *versus* DCF fluorescence.

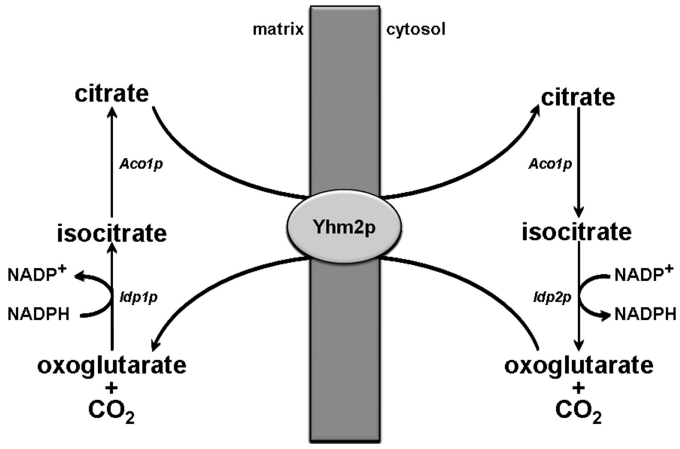

FIGURE 12. **Scheme of the reactions involved in the citrate-oxoglutarate NADPH shuttle from the mitochondrial matrix to the cytosol in *S. cerevisiae*.**

mercurials, *N*-ethylmaleimide and tannic acid, in contrast to CTP and Ctp1p. In addition, Yhm2p shares only 21 and 22% identical amino acids with Ctp1p and CTP, respectively. Yhm2p also differs from the dicarboxylate (38, 39) and oxaloacetate (16, 40) carriers that transport malate and phosphate, oxaloacetate and sulfate, respectively, as principal substrates and do not transport citrate, oxoglutarate, and fumarate.

Apart from the relatively low homology that Yhm2p shares with transporters for carboxylates, Dic1p (24% of identical amino acids), Sfc1p (23%), Oac1p (21%), Ctp1p (21%), and Odc1p (20%), Yhm2p does not exhibit significant sequence homology with any other MC functionally identified so far greater than the basic homology existing between the different members of the MC family. However, several proteins encoded by the genomes of fungi are very likely orthologs of Yhm2p. These sequences include the following: XP_448544.1 from *Candida glabrata* (88% of identical amino acids with Yhm2p); XP_001385050.2 from *Pichia stipitis* (74%); XP_001523814.1 from *Lodderomyces elongisporus* (73%); XP_747921.1 from *Aspergillus fumigatus* (72%); XP_001266111.1 from *Neosartorya fischeri* (71%); XP_002149092.1 from *Penicillium marneffei* (71%); XP_461777.1 from *Debaryomyces hansenii* (71%); XP_001242399.1 from *Coccidioides immitis* (71%); XP_956895.1 from *Neurospora crassa* (70%); ACF20293.1 from *Fusarium oxysporum* (69%); XP_001228268.1 from *Chaetomium globosum* (65%); XP_568307.1 from *Cryptococcus neoformans* (62%); and NP_595645.1 from *Schizosaccharomyces pombe* (56%). Moreover, reciprocal BLASTP revealed the existence of putative orthologs of Yhm2p in Alveolata (*e.g.* XP_001350635.1 from *Plasmodium falciparum* (31%) and XP_001238657.1 from *Eimeria tenella* (31%)), Euglenozoa (*e.g.* XP_811279.1 from *Trypanosoma cruzi* (32%)), and Stramenopiles (*e.g.* XP_002180033.1 from *Phaeodactylum tricornutum* (29%)), despite their low percentage of identical amino acids with Yhm2p. On the contrary, it is unlikely that there is an orthologous Yhm2p carrier in higher eukaryotes.

As we have found an accumulation of citrate in Δ*YHM2* cell mitochondria, Yhm2p appears to be essential for the export of citrate from the mitochondria to the cytosol, at least under the experimental conditions employed in this study. In the cytosol, citrate can be used, via isocitrate, to produce oxoglutarate and NADPH by the action of the $NADP^+$-dependent cytosolic isocitrate dehydrogenase, Idp2p (Fig. 12). Therefore, a primary physiological function of Yhm2p is to increase cytosolic NADPH, which is required for various biosynthetic reactions and thiol-dependent peroxidases that utilize reduced glutathione or thioredoxin to protect the cell from oxidative damage. Moreover, because Yhm2p functions exclusively by antiport and oxoglutarate is efficiently transported by this carrier, oxoglutarate can enter the mitochondria in exchange for citrate via Yhm2p. In mitochondria, oxoglutarate can be converted to isocitrate by the $NADP^+$-dependent mitochondrial isocitrate dehydrogenase, Idp1p, and then to citrate, leading to net export of NADPH-reducing equivalents (Fig. 12). Thus, Yhm2p may act as a key component of the citrate-oxoglutarate NADPH redox shuttle between mitochondria and cytosol.

The experimental data reported in this study shed light on the physiological role of Yhm2p. The observed decrease in the NADPH/$NADP^+$ ratio in the cytosol of Δ*YHM2* cells, compared with that in wild-type cells, as well as its more pronounced decrease in the cytosol of H_2O_2-treated Δ*YHM2* cells strongly support the important function of Yhm2p to increase the redox state of cytosolic NADPH. The consequent antioxidant function of Yhm2p is further substantiated by the decreased GSH/GSSG ratio in the cytosol of Δ*YHM2* cells with and without treatment of H_2O_2. In addition, the marked increase in the NADPH/$NADP^+$ ratio in the mitochondria of H_2O_2-treated Δ*YHM2* and Δ*YHM2*Δ*ZWF1* cells, along with the reduction in this ratio in the cytosol of the above cells, suggest that Yhm2p is involved in shuttling NADPH reducing equivalents from the mitochondrial matrix to the cytosol.

In wild-type *S. cerevisiae* cells grown in acetate-supplemented SC, H_2O_2-induced oxidative stress is counteracted by endogenous antioxidants. Unlike wild-type cells, Δ*YHM2* cells exhibit a growth defect when treated with H_2O_2, because upon addition of exogenous ROS, the antioxidant ability of the cell is overcome. Therefore, the sensitivity of the Δ*YHM2* null mutant to H_2O_2 also lends support to the antioxidant role of Yhm2p. It is worth mentioning that the sensitivity of the Δ*YHM2* strain to H_2O_2 parallels the earlier observations that *S. cerevisiae* cells lacking Idp2p or Zwf1p (*i.e.* major sources of cytosolic NADPH) are sensitive to the oxidant agent H_2O_2 (41, 42). Furthermore, in the absence of exogenous oxidants, yeast cells lacking both the *ZWF1* and *IDP2* genes display a dramatic growth defect when shifted from glucose to acetate (41, 43). This defect was found to be correlated to increased levels of intracellular oxidants produced during acetate metabolism (41, 43). Consistently, our results show that the ROS level is enhanced in Δ*YHM2* cells and more so in Δ*YHM2*Δ*ZWF1* cells.

In this investigation, Δ*YHM2* yeast cells have been compared with Δ*ZWF1*, Δ*YHM2*Δ*ZWF1*, and Δ*CTP1* cells. As observed for the Δ*YHM2* strain, the *ZWF1*-deleted strain exhibits a decrease in the cytosolic NADPH/$NADP^+$ and GSH/GSSG ratios, which is more evident in the presence of H_2O_2. In addition, and importantly, the combination of *YHM2* and *ZWF1* deletions causes a more pronounced H_2O_2-induced growth defect that is consistent with the greater decrease in the NADPH/$NADP^+$ ratio. The cytosolic GSH/GSSG ratio is also diminished in Δ*ZWF1* and Δ*YHM2*Δ*ZWF1* strains as compared with the wild-type strain, although in the presence of H_2O_2 substantial protein glutathionylation and *ex novo* synthesis of glutathione take place. In light of our observations whereby no significant variations in the NADPH/$NADP^+$ and GSH/GSSG ratios occur in Δ*CTP1* cells in contrast to Δ*YHM2* cells, it appears that Ctp1p, the known citrate/malate transporter of *S. cerevisiae* (26), cannot substitute the antioxidant function of Yhm2p. Although the contrasting ability of Ctp1p and Yhm2p to increase the redox state of cytosolic NADPH and GSH requires further investigation, it should be noted that Ctp1p does not transport oxoglutarate (26, 44) accounting, at least in part, for the differences observed. Specifically, in Δ*YHM2* cells, oxoglutarate is unable to enter the mitochondria in exchange for citrate and regenerate this substrate inside the organelles via the action of Idp1p and Aco1p (Fig. 12). Indeed, Δ*YHM2* and especially Δ*YHM2*Δ*ZWF1* strains display an increase in cytosolic oxoglutarate, which is not observed in the presence of H_2O_2 because under severe oxidative stress oxoglutarate is mainly used to produce GSH. Moreover, Δ*CTP1* was found to be the yeast strain most resistant to paraquat (a reagent widely used to produce superoxide in cells and mitochondria) among the 29 tested strains, each lacking a gene for proven or putative MCs (45).

Interestingly, two isocitrate-oxoglutarate NADPH redox shuttles have been proposed to exist in mammals as follows: the first to keep intraperoxisomal $NADP^+$ reduced (46), and the second to equilibrate the cytosolic and mitochondrial $NADP^+$ redox potentials (47, 48 and references therein). The former involves a characterized (but not yet identified) isocitrate-oxoglutarate transport system of the peroxisomal membrane (46) and the latter the mammalian citrate/malate (25) and oxoglutarate/malate (49) carriers of the mitochondrial membrane. Our findings suggest the existence of a Yhm2p-dependent mitochondrial NADPH redox shuttle in *S. cerevisiae*, which is capable of reducing $NADP^+$ in the cytosol; this reducing power is required for the functioning of biosynthetic and antioxidant reactions. It will be of interest to investigate in future studies whether there are conditions in which the NADPH shuttle of yeast mitochondria operates in the reverse direction, *i.e.* transferring NADPH-reducing equivalents from the cytosol to the mitochondria. These studies would ascertain whether the NADPH shuttle cooperates with the NADH kinase Pos5p and the acetaldehyde dehydrogenase Ald4p to produce intramitochondrial NADPH, which is essential for several processes, such as ROS scavenging, iron homeostasis, and fatty acid and arginine biosynthesis (50, 51).

REFERENCES

1. Cho, J. H., Ha, S. J., Kao, L. R., Megraw, T. L., and Chae, C. B. (1998) *Mol. Cell. Biol.* **18,** 5712–5723
2. MacAlpine, D. M., Perlman, P. S., and Butow, R. A. (1998) *Proc. Natl. Acad. Sci. U.S.A.* **95,** 6739–6743
3. Palmieri, F. (2004) *Pflugers Arch.* **447,** 689–709
4. Palmieri, F. (2008) *Biochim. Biophys. Acta* **1777,** 564–578
5. Palmieri, F., and Pierri, C. L. (2010) *FEBS Lett.* **584,** 1931–1939
6. Palmieri, F., Agrimi, G., Blanco, E., Castegna, A., Di Noia, M. A., Iacobazzi, V., Lasorsa, F. M., Marobbio, C. M., Palmieri, L., Scarcia, P., Todisco, S., Vozza, A., and Walker, J. (2006) *Biochim. Biophys. Acta* **1757,** 1249–1262
7. Baudin, A., Ozier-Kalogeropoulos, O., Denouel, A., Lacroute, F., and Cullin, C. (1993) *Nucleic Acids Res.* **21,** 3329–3330
8. Güldener, U., Heck, S., Fielder, T., Beinhauer, J., and Hegemann, J. H. (1996) *Nucleic Acids Res.* **24,** 2519–2524
9. Goldstein, A. L., and McCusker, J. H. (1999) *Yeast* **15,** 1541–1553
10. Sherman, F. (1991) *Methods Enzymol.* **194,** 3–21
11. Daum, G., Gasser, S. M., and Schatz, G. (1982) *J. Biol. Chem.* **257,** 13075–13080
12. Palmieri, F., Indiveri, C., Bisaccia, F., and Iacobazzi, V. (1995) *Methods Enzymol.* **260,** 349–369
13. Fiermonte, G., Walker, J. E., and Palmieri, F. (1993) *Biochem. J.* **294,** 293–299
14. Palmieri, L., Pardo, B., Lasorsa, F. M., del Arco, A., Kobayashi, K., Iijima, M., Runswick, M. J., Walker, J. E., Saheki, T., Satrústegui, J., and Palmieri, F. (2001) *EMBO J.* **20,** 5060–5069
15. Todisco, S., Agrimi, G., Castegna, A., and Palmieri, F. (2006) *J. Biol. Chem.* **281,** 1524–1531
16. Marobbio, C. M., Giannuzzi, G., Paradies, E., Pierri, C. L., and Palmieri, F. (2008) *J. Biol. Chem.* **283,** 28445–28453

17. Wang, H., and Joseph, J. A. (1999) *Free Radic. Biol. Med.* **27,** 612–616
18. Halliwell, B., and Whiteman, M. (2004) *Br. J. Pharmacol.* **142,** 231–255
19. Salmon, T. B., Evert, B. A., Song, B., and Doetsch, P. W. (2004) *Nucleic Acids Res.* **32,** 3712–3723
20. Wang, X., Perez, E., Liu, R., Yan, L. J., Mallet, R. T., and Yang, S. H. (2007) *Brain Res.* **1132,** 1–9
21. Fearnley, I. M., Carroll, J., Shannon, R. J., Runswick, M. J., Walker, J. E., and Hirst, J. (2001) *J. Biol. Chem.* **276,** 38345–38348
22. Fiermonte, G., Dolce, V., and Palmieri, F. (1998) *J. Biol. Chem.* **273,** 22782–22787
23. St. John, P. A., Kell, W. M., Mazzetta, J. S., Lange, G. D., and Barker, J. L. (1986) *J. Neurosci.* **6,** 1492–1512
24. Robinson, A. J., and Kunji, E. R. (2006) *Proc. Natl. Acad. Sci. U.S.A.* **103,** 2617–2622
25. Kaplan, R. S., Mayor, J. A., and Wood, D. O. (1993) *J. Biol. Chem.* **268,** 13682–13690
26. Kaplan, R. S., Mayor, J. A., Gremse, D. A., and Wood, D. O. (1995) *J. Biol. Chem.* **270,** 4108–4114
27. Palmieri, F., Stipani, I., Quagliariello, E., and Klingenberg, M. (1972) *Eur. J. Biochem.* **26,** 587–594
28. Bisaccia, F., De Palma, A., and Palmieri, F. (1989) *Biochim. Biophys. Acta* **977,** 171–176
29. Klingenberg, M. (1989) *Arch. Biochem. Biophys.* **270,** 1–14
30. Henke, B., Girzalsky, W., Berteaux-Lecellier, V., and Erdmann, R. (1998) *J. Biol. Chem.* **273,** 3702–3711
31. van Roermund, C. W., Hettema, E. H., Kal, A. J., van den Berg, M., Tabak, H. F., and Wanders, R. J. (1998) *EMBO J.* **17,** 677–687
32. Schäfer, H., Nau, K., Sickmann, A., Erdmann, R., and Meyer, H. E. (2001) *Electrophoresis* **22,** 2955–2968
33. Mozdy, A. D., McCaffery, J. M., and Shaw, J. M. (2000) *J. Cell. Biol.* **151,** 367–380
34. Wells, G. B., Dickson, R. C., and Lester, R. L. (1998) *J. Biol. Chem.* **273,** 7235–7243
35. Pinto, W. J., Srinivasan, B., Shepherd, S., Schmidt, A., Dickson, R. C., and Lester, R. L. (1992) *J. Bacteriol.* **174,** 2565–2574
36. el Moualij, B., Duyckaerts, C., Lamotte-Brasseur, J., and Sluse, F. E. (1997) *Yeast* **13,** 573–581
37. Nelson, D. R., Felix, C. M., and Swanson, J. M. (1998) *J. Mol. Biol.* **277,** 285–308
38. Palmieri, L., Palmieri, F., Runswick, M. J., and Walker, J. E. (1996) *FEBS Lett.* **399,** 299–302
39. Fiermonte, G., Palmieri, L., Dolce, V., Lasorsa, F. M., Palmieri, F., Runswick, M. J., and Walker, J. E. (1998) *J. Biol. Chem.* **273,** 24754–24759
40. Palmieri, L., Vozza, A., Agrimi, G., De Marco, V., Runswick, M. J., Palmieri, F., and Walker, J. E. (1999) *J. Biol. Chem.* **274,** 22184–22190
41. Minard, K. I., and McAlister-Henn, L. (1999) *J. Biol. Chem.* **274,** 3402–3406
42. Minard, K. I., and McAlister-Henn, L. (2005) *J. Biol. Chem.* **280,** 39890–39896
43. Minard, K. I., and McAlister-Henn, L. (2001) *Free Radic. Biol. Med.* **31,** 832–843
44. Evans, C. T., Scragg, A. H., and Ratledge, C. (1983) *Eur. J. Biochem.* **130,** 195–204
45. Cochemé, H. M., and Murphy, M. P. (2008) *J. Biol. Chem.* **283,** 1786–1798
46. Visser, W. F., van Roermund, C. W., Ijlst, L., Hellingwerf, K. J., Waterham, H. R., and Wanders, R. J. (2006) *Biochem. Biophys. Res. Commun.* **348,** 1224–1231
47. Hoek, J. B., and Ernster, L. (1974) in *Alcohol and Aldehyde Metabolizing Systems* (Thurman, R. G., Yonetani, T., Williamson, J. R., and Chance, B., eds) pp. 351–364, Academic Press, Inc., New York
48. Williamson, J. R., and Cooper, R. H. (1980) *FEBS Lett.* **117,** K73–K85
49. Runswick, M. J., Walker, J. E., Bisaccia, F., Iacobazzi, V., and Palmieri, F. (1990) *Biochemistry.* **29,** 11033–11040
50. Outten, C. E., and Culotta, V. C. (2003) *EMBO J.* **22,** 2015–2024
51. Hiltunen, J. K., Schonauer, M. S., Autio, K. J., Mittelmeier, T. M., Kastaniotis, A. J., and Dieckmann, C. L. (2009) *J. Biol. Chem.* **284,** 9011–9015